HOSTED BY
ELSEVIER
Available online at www.sciencedirect.com
ScienceDirect
Soils and Foundations 63 (2023) 101398
www.elsevier.com/locate/sandf

Technical Paper

Behavior of multi-layer permeable reactive barriers for groundwater remediation

Stefania Bilardi, Silvia Simonetti, Paolo Salvatore Calabrò, Nicola Moraci *

Department of Civil, Energy, Environmental and Material Engineering (DICEAM), Mediterranea University of Reggio Calabria, Via Graziella loc. Feo di Vito, 89122 Reggio Calabria, Italy

Received 17 January 2023; received in revised form 6 September 2023; accepted 31 October 2023
Available online 20 November 2023

Abstract

This paper aims to evaluate the efficiency of a multilayer configuration of a permeable reactive barrier (PRB) made up of granular mixtures of zero valent iron (ZVI) and lapillus. The latter is a volcanic material used to disperse ZVI particles. A high dispersion of ZVI improves the long-term hydraulic conductivity but can significantly reduce reactivity due to the lower amount of ZVI. In this research, the performance of two different combinations of a two-layer configuration was studied by means of long-term column tests. The first layer, named "pre-treatment layer", had a thickness of 4 cm and a volumetric ratio (ZVI/lapillus) of 10:90 or 05:95, while the second layer had a volumetric ratio (ZVI/lapillus) of 20:80. A single layer configuration made only of the 20:80 ZVI/lapillus was used as a benchmark. The three tests were performed using a multi-contaminated solution of copper, nickel and zinc. Test results showed an early loss of the hydraulic conductivity in the single layer configuration and an increase of PRB longevity by 68 % in the presence of the pre-treatment layer. The pre-treatment zone containing 10 % ZVI delayed the clogging phenomenon, while the zone with 5 % ZVI ensured both the correct long-term hydraulic behavior and a removal efficiency higher than 77.6 % for Nickel and 99 % for copper and zinc at 23 cm of thickness for at least two months.

Keywords: Copper; Hydraulic conductivity; Iron corrosion; Nickel; Permeable reactive barrier; Lapillus; Zinc

1. Introduction

Groundwater contamination from heavy metals has a significant impact on the ecosystem and human health due to the high level of toxicity of metals mainly released into the environment by industrial activities or uncontrolled waste disposal (Rajendran et al., 2022). Today groundwater remediation requires the use of sustainable technologies able to reduce greenhouse gas emissions during their implementation and operation and capacity of guaranteeing the drinking and/or agricultural uses of the water resource. A permeable reactive barrier (PRB) can represent a solution to this issue. A PRB involves placing a reactive and permeable medium into the aquifer to intercept the contaminated plume, without energy input but using the natural hydraulic gradient, and to stop the contaminant propagation (Obiri-Nyarko et al., 2014; Thakur et al., 2020).

Singh et al. (2020) defined "multi-PRB" as a sequence of two or more barriers composed of different reactive media or a single barrier made up of different layers, the latter configuration is also known as multi-layer PRB (Lee et al., 2010; Pawluk et al., 2019; Pawluk and Fronczyk, 2015; Połoński et al., 2017; Xu et al., 2012; Ye et al., 2019). Both configurations were mainly proposed to tackle a complex contamination by using different materials

* Corresponding author at: Via Graziella loc. Feo di Vito 89122, Reggio Calabria, Italy.
E-mail address: nicola.moraci@unirc.it (N. Moraci).

https://doi.org/10.1016/j.sandf.2023.101398

which can be able to activate specific removal mechanisms for the different contaminants.

The longevity (i.e. the time during which the barrier guarantees reaching remediation goals without replacing the reactive medium) is an important requirement for a PRB and it can be achieved by using one or more reactive media with suitable characteristics of reactivity and permeability to treat the contamination in the long term. Longevity increases PRB sustainability avoiding the costs and impacts related to substitution and disposal of the exhausted reactive medium during remediation. In terms of PRB sustainability, the use of cheap and readily available materials is also desirable (avoiding excessive costs and transport over long distances), derived from sustainable production processes or from waste products (Calabrò et al., 2021). In this context, zero valent iron (ZVI), a versatile reactive medium supplied by different manufacturers, known and used worldwide in laboratory or in full scale PRB meets all the requirements aforementioned (Fu et al., 2014; Makota et al., 2017; Ullah et al., 2020a; Zhu et al., 2022). Although there are examples of a good longevity of this reactive medium in full scale (Wilkin et al., 2014), there are numerous cases when a significant reduction of the barrier permeability occurred (Henderson and Demond, 2007). This phenomenon is mainly caused by the formation of iron oxides and hydroxides which, due to their expansive nature, reduce the porosity and permeability of the barrier (Cao et al., 2021; Hu et al., 2018). Mixing ZVI with another granular medium is a well-established strategy to prevent permeability reduction (Bilardi et al., 2020; Hu et al., 2020; Moraci et al., 2017, 2015; Ruhl et al., 2014). The role of the admixing agent, such as sand or volcanic materials (e.g. pumice, lapillus, zeolites), is to separate iron particles and prevent the aggregation of ZVI particles from following their expansion which can cause clogging phenomena (Hu and Noubactep, 2019; Hu et al., 2020; Limper et al., 2018; Ullah et al., 2020b; Yang et al., 2022). The dispersion rate of ZVI cannot be established a priori since the iron corrosion process, and the resulting formation of its corrosion products, depends on the aquifer characteristics (e.g. groundwater chemical composition and flow velocity (Madaffari et al., 2017)).

Clogging in a ZVI-PRB generally occurs at the inlet section of the barrier (ITRC, 2011; Phillips et al., 2010; Ullah et al., 2020b; Yang et al., 2016). To tackle this issue, a multi-layer configuration was proposed in literature and implemented in full scale PRBs (Gavaskar et al., 2000; Li and Benson, 2010; Morrison, 2003). The multi-layer configuration consists of two layers: the first containing ZVI mixed with an inert material (e.g. sand or gravel) and the second composed of ZVI only. The first layer was called pre-treatment layer or "sacrificial pre-treatment zone" (Li and Benson, 2010) since its scope is to preserve the permeability of the reactive zone of the barrier by chemically pretreating the groundwater.

An example of this configuration is at Monticello, UT, USA (Morrison, 2003), where a pre-treatment zone 0.6 m thick (13 % of ZVI and 87 % gravel by volume) was placed upstream of the reactive zone, 1.2 m thick, composed of 100 % ZVI and of a third zone, 0.6 m thick, composed of crushed gravel with the function of distributing the treated water to the aquifer. Field studies have documented the greatest loss of hydraulic conductivity occurring within the center of the 100 % ZVI zone (Bartlett, 2005). Much of the decrease was attributed to precipitation of calcium carbonate and other ZVI corrosion products (Li and Benson, 2010; Morrison, 2003).

A multi-layer PRB was also installed is at Dover Air Force Base, DE, USA where the pre-treatment zone (10 % of ZVI and 90 % coarse sand by volume and 0.6 m thick) precedes the ZVI reactive zone. As in the Monticello site, the exit zone consists of 100 % coarse sand. The pre-treatment zone was installed to limit the entry of oxygen into the reactive zone and monitoring after 18 months confirmed its depletion before entering the reactive cell. This indicates that by incorporating a pre-treatment zone upstream the real reactive one may improve barrier longevity (Gavaskar et al., 2000).

Li and Benson (2010) numerically studied the efficiency of a pre-treatment zone by means of a ground water flow model MODFLOW and reactive transport model RT3D. The aim of the pre-treatment layer is to create a zone to promote secondary mineral formation due to pH and redox change before groundwater enters the reactive zone. According to the results obtained by the authors, a pre-treatment zone does not eliminate the reduction in porosity completely, as secondary minerals (e.g., $Fe(OH)_2$) still form within the reactive zone in response to iron corrosion.

The in situ experiences described above and the modelling study revealed how a pre-treatment zone does not exclude the occurrence of clogging phenomena and, according to the Authors, this aspect should be studied in greater depth. Therefore, a configuration indicated here as multi-layer configuration and composed of granular mixtures characterized by a different degree of iron dispersion, is investigated in this paper, since, based on the authors' knowledge, this configuration has not yet been studied in scientific literature. The rationale of this configuration is to use a greater dispersion of the iron in the first layer of the barrier where the higher polluting load or the presence of oxygen could increase iron corrosion and, therefore, the risk of clogging phenomena (Bilardi et al., 2019). This zone should promote secondary minerals and the formation of iron corrosion products avoiding clogging phenomena. Whereas, the lower dispersion of the ZVI in the second layer should assure greater longevity of the barrier in terms of reactivity, while ensuring the permeability necessary for groundwater flow.

This paper studies the performance of two-layer configurations using different ZVI/lapillus mixtures by means column tests. Lapillus was chosen as it is cheap, widely available all over the world and has a moderate adsorption capacity (Bilardi et al., 2020). In the first layer (pre-treatment layer), 4 cm thick, the volumetric ratio (V.R.)

ZVI:lapillus adopted is either 10:90 (Column B) or 05:95 (Column C), whereas in the second layer a mixture with a volumetric ratio of 20:80 is used. A single layer configuration made of a 20:80 ZVI/lapillus mixture (Column A) is used as a benchmark. The results of the three column tests are compared in terms of variation over time and over the barrier thickness of the hydraulic conductivity and the normalized contaminant concentration towards a multi-contaminated solution of copper, nickel and zinc. This composition could be representative of a contamination of industrial origin. It reflects a serious scenario, because nickel is toxic, even at low concentrations, as well as being difficult and complex to remove because nickel and zinc removal is negatively affected by the presence of copper (Bilardi et al., 2019).

2. Materials and methods

2.1. ZVI and lapillus

The ZVI used is of the FERBLAST RI 850/3.5 type, distributed by Pometon S.p.A., Mestre, Italy. The material is mainly made of iron (>99.74 %) and impurities include Mn, O, S and C. As derived from grain size analysis, the mean grain size (*d50*) is about 0.5 mm and the coefficient of uniformity (*U*) is 2. The particle density of the reactive material is 7.87 g/cm^3.

Lapillus is a sedimentary pyroclastic material with a granular form and a reddish-maroon color. It originated from the explosive volcanic activity in the Sabatini Mountains (Italy) and is distributed by "Società Estrattiva Monterosi s.r.l.", Viterbo, Italy. Lapillus mainly consists of silica (SiO_2, 47 % mass) and oxides of various elements (Al_2O_3, 15 %; K_2O, 8 %; Na_2O, 1 %; Fe_2O_3-FeO, 7–8 %; MnO, 0.15 %; MgO, 5.5 % and CaO, 11 %). The grain size distribution of Lapillus specimen used in column tests has been selected in function of that of ZVI and taking into consideration the internal stability filter design criteria (Moraci et al., 2022). The lapillus grains were washed, the retained grains in sieve No. 40 (>0.42 mm) and the passing to sieve No. 200 (<0.074 mm) were discarded in order to obtain a particle size distribution more similar to that of ZVI. The coefficient of uniformity *U* is about 3.2 and the *d50* is approximately 0.4 mm. The apparent particle density of the lapillus is 2.2 g/ cm^3.

The two materials with a bulk density of 4 g/cm^3 for ZVI and of 1.27 g/cm^3 for lapillus were mixed in such a way as to obtain volumetric ratios equal to 05:95; 10:90 and 20:80, which are equivalent to the weight ratios of 44:56, 26:74, 14:86, respectively.

2.2. Column tests

Laboratory scale polymethyl methacrylate (Plexiglas) columns were used in this research. Column tests were carried out in up-flow mode under constant flow rate of 0.5 mL/min (*Q*) using a multi-channel precision peristaltic pump (Watson Marlow 205S). The columns, with an internal diameter of 5 ± 0.1 cm and height equal to 50 cm, were half filled and the concentration profile of the contaminants was obtained from the sampling ports located at distance of 3, 5, 8, 13, 18, 23 and 28 cm from inlet. A schematic diagram of column test apparatus is showed in Fig. 1.

To obtain a specimen as homogeneous as possible, each column was filled by means of a tube containing the reactive medium, inserted inside the column and gently lifted during filling. The material was compacted by gently tapping the outside of the column with a rubber hammer. The columns were filled up to about 28 cm, a width sufficient to study the propagation of the contamination front (Bilardi et al., 2023); the empty area of the columns was filled with quartz gravel.

The contaminated solution was prepared by diluting Copper Nitrate (Copper(II) nitrate hydrate, purity > 99 %; Sigma-Aldrich), Nickel Nitrate (Nickel(II) nitrate hexahydrate, purity > 99 %; Sigma-Aldrich) and Zinc Nitrate (Zinc(II) nitrate hexahydrate, purity > 99 %; Sigma-Aldrich) in distilled water in order to obtain a concentration of about 18 mg/l for each metal.

The aqueous samples withdrawn from sampling ports were analysing using Inductively Coupled Plasma – Optical Emission Spectroscopy (ICP-OES - Perkin Elmer Optima 8000).

The hydraulic behaviour was studied through pressure transducers (TE Connectivity US300, pressure range of 0 – 200 kPa, ± 0.1 % accuracy). Each pressure transducer was connected to an automated data logger to record pressure values. The difference of pressure between a first transducer located before the column inlet and a second one located at 3 cm from column inlet (Fig. 1), allowed the authors to determine the hydraulic conductivity of the first layer (or "pre-treatment layer) of the reactive medium. The difference of pressure between the second and the third pressure traducer, the latter located at 25 cm from column inlet (Fig. 1), allowed the determination of the hydraulic conductivity of the remaining part of the reactive medium. The hydraulic conductivity (*k*) of the specimen was calculated in accordance with the following form of Darcy's law:

$$k = \frac{L \cdot Q}{\Delta H \cdot A} \tag{1}$$

where *A* is the area of the column, *L* is the length of the specimen and ΔH is the hydraulic head loss.

Finally, the material extracted from columns at the end of the test, was analysed by Scanning Electron Microscopy (SEM) coupled with Energy Dispersion X-ray Spectroscope (EDX) in order to evaluate the morphology of the reaction products and their elemental composition.

Table 1 summarizes the main characteristic of the column tests performed considering a single layer (Column A) of the ZVI/lapillus mixture at a volumetric ratio equal to 20:80, or a double layer with a volumetric ratio equal to 10:90 and 20:80 for the second layer (Column B) or 05:95 for the first layer and 20:80 for the second layer (Col-

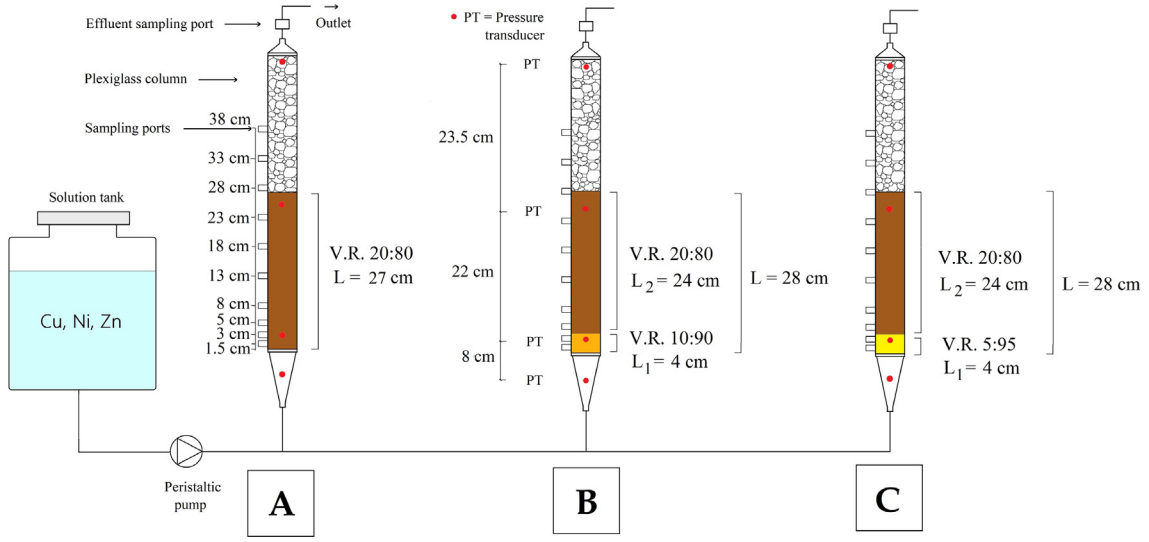

Fig. 1. Schematic diagram of column tests.

Table 1
Main characteristic of column tests.

		A	B	C
First layer	V.R. ZVI/lapillus	20:80	10:90	05:95
	Thickness (cm)	4	4	4
	ZVI mass (g)	63	31	16
	Lapillus mass (g)	80	90	95
Second layer	V.R. ZVI/lapillus	20:80	20:80	20:80
	Thickness (cm)	23	24	24
	ZVI mass (g)	361	377	377
	Lapillus mass (g)	459	479	479
Total thickness (cm)		27	28	28
Initial porosity (%)		43.6	43.2	43.0
Initial hydraulic conductivity (m/s)		$2.38 \cdot 10^{-4}$	$2.77 \cdot 10^{-4}$	$1.64 \cdot 10^{-4}$
Test duration (h)		3144	6360	7932

umn C). The rationale of this configuration is to use a higher dispersion of the ZVI in the first layer, in order to reduce the risk of clogging phenomena, and a lower dispersion of ZVI in the second layer in order to assure greater longevity in terms of reactivity, while ensuring the permeability necessary for groundwater flow. Moreover, Table 1 shows the initial porosity (n_0) and the hydraulic conductivity value of the three specimens and the duration of the three tests. The A column test was interrupted after 131 days due to the reduction in the hydraulic conductivity which was not compatible with the imposed flow rate. The B and C column tests were interrupted after 265 and 330 days, respectively, due to exhaustion of the reactivity.

3. Results and discussion

A PRB loses its effectiveness if it does not guarantee a concentration of the contaminant leaving the PRB below the remediation target or when its hydraulic conductivity decreases and groundwater flow is unable to cross the barrier. Therefore, the longevity of the barrier will be established by examining the hydraulic and the reactive behavior of the three columns.

3.1. Hydraulic behavior

Fig. 2 illustrates the hydraulic conductivity calculated at time t ($k(t)$) divided by the initial value (k_0) of the first (0–3 cm) and second layer (3–25 cm) of the three columns as a function of time. The single layer configuration (Column A) shows the lowest longevity. In particular, the hydraulic conductivity of the first layer (Fig. 2a) decreases abruptly after about 200 and 1000 h for columns A and B respectively. For column C, the hydraulic conductivity remains constant up to 3000 h and subsequently a slight increase is observed, the latter probably due to gas venting or to the formation and removal of solids precipitates.

With reference to the second layer (Fig. 2b), the hydraulic conductivity decreases after 1600 h for column A,

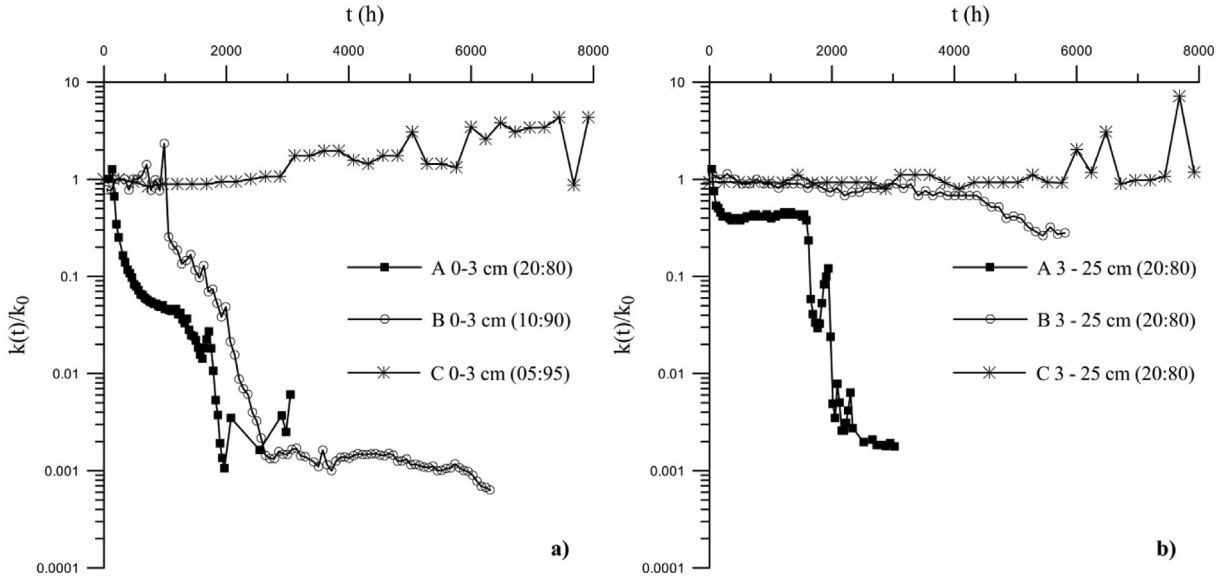

Fig. 2. Normalized hydraulic conductivity profile of a) the first (0–3 cm) and b) second (3–25 cm) layer of the reactive media contained in columns A, B and C.

slightly decreases after 4200 h for column tests B, whereas it remains constant for column test C.

As expected, column A shows the worst hydraulic behavior, in fact, a rapid reduction in the hydraulic conductivity starting from the column inlet is observed. Therefore, considering the examined condition of flow rate and water composition, this configuration does not ensure the correct operation of the PRB.

The hydraulic conductivity profile of the first layer of column B is almost the same as that observed in column A, but the reduction in the hydraulic conductivity occurs later due to the lower iron content per unit volume. This strong similarity of the hydraulic conductivity profile of the first layer of columns B and A suggests a very precise kinetics of iron corrosion under the same boundary conditions (i.e. flow rate and water composition).

Examining columns B and C it is possible to state that a "pre-treatment" layer improves the long-term hydraulic behavior of the PRB and can preserve the hydraulic conductivity of the subsequent layer. The different hydraulic behavior of the second layer of the three column tests is probably due to the presence of the "pre-treatment" zone that changes the chemical composition of the water flow entering the second layer.

As pointed out by Hu et al. (2020) the solution chemistry influencing iron corrosion rate includes the presence of dissolved O_2 (probably consumed in the pretreatment zone) and contaminants whose removal starts from this zone. Another important concept pointed out by the same authors (Hu et al., 2020) is the nonlinear kinetic of iron corrosion rate.

3.2. Reactive behavior

Fig. 3 shows the breakthrough curves (i.e. profile of the normalized concentration of the heavy metals over time) at the second sampling port (3 cm) for the three column tests. The removal sequence Cu > Zn > Ni confirms the results observed in previous research (Bilardi et al., 2019, 2015). Examining copper removal (Fig. 3a), the breakthrough time (i.e. the time the system is able to keep the concentration of the pollutant below the Italian regulatory limit (i.e. 1 mg/L)) is similar for columns B (i.e. 3696 h) and C (i.e. 3528 h). The breakthrough time was never reached for column A which had a shorter duration due to the excessive reduction in hydraulic conductivity. The breakthrough curves for nickel (Fig. 3b) and zinc (Fig. 3c) vary for the three columns and the highest removal of the contaminant is achieved as the iron content per unit volume increases. In particular, the Italian regulatory limit for nickel (i.e. 0.02 mg/L) is always exceeded in the three columns. For Zinc, the Italian regulatory limit (i.e. 3 mg/L) is exceeded after 672 h for column A, after 336 h for column B and starting from the first sampling (i.e. 168 h) for column C.

The complete exhaustion (i.e. $C(t)/C_0$ equal to 1) of the reactive medium towards copper is not observed in the three columns where the removal efficiency is always higher than 70 %. While the complete exhaustion of the reactive medium in the first 3 cm of thickness towards nickel and zinc is observed only for column C.

It is possible to observe a relation between the hydraulic (Fig. 2) and reactive behavior (Fig. 3). The cause of the reduction in hydraulic conductivity observed in columns A and B (Fig. 2) can be attributed to the formation of iron corrosion products, which probably contribute to the residual removal of nickel and zinc by co-precipitation (i.e. dissolved species are mechanically entrapped in the matrix of oxyhydroxides during their precipitation) and adsorption onto available iron oxides (Fig. 3b and 3c). The constant value of the hydraulic conductivity (Fig. 2) and the complete exhaustion of the first layer of column C in the long

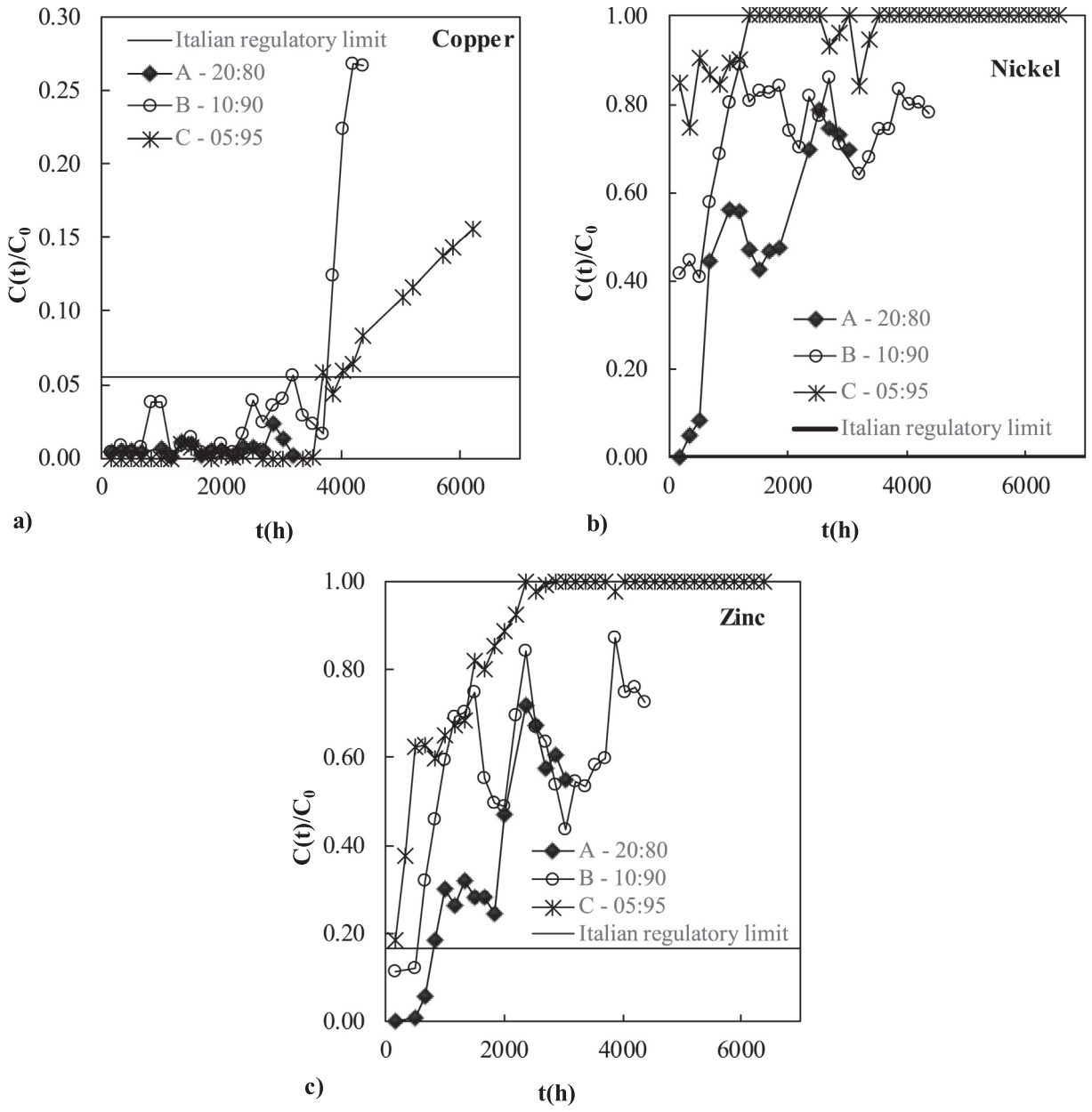

Fig. 3. Breakthrough curves of a) copper b) nickel and c) zinc at the second sampling port (3 cm) of columns A, B and C.

term (Fig. 3a and 3c) suggests a lower formation of iron corrosion products and the consequent reduction of the heavy metal removal capacity.

Fig. 4 shows the breakthrough curves of nickel (Fig. 4a) and zinc (Fig. 4b) derived from column test A. Because in all sampling ports located after 3 cm, copper concentration remained below 1 mg/l, the breakthrough curves related to copper are not showed.

The breakthrough time, which is the design parameter of a PRB (Bilardi et al., 2019), is considered the length of time the system is able to keep the concentration of the pollutant below the Italian regulatory limit. For nickel (Fig. 4a), the breakthrough time is observed at 5 cm of the reactive medium thickness after 504 h, and it occurs at the same time (i.e. 2520 h) at the sampling ports located at 13, 18 and 23 cm. In terms of pore volume of flow (PVF), calculated through equation (2), the breakthrough time at L = 5 cm (i.e. t = 504 h) occurred after 353 PVF and at L = 13 cm, L = 18 cm and L = 23 cm (i.e. t = 2520 h) after 679, 491 and 384 PVF respectively.

$$PVF = \frac{Q \cdot t}{A \cdot n_0 \cdot L} \tag{2}$$

Regarding Zinc removal, its concentration at a thickness L = 23 cm is lower than the Italian regulatory limit for the entire duration of the test. The breakthrough time observed at sampling ports located at 3 (Fig. 3c), 5, 8 and 13 cm linearly increases with the reactive medium thickness as will be shown later in Fig. 7b.

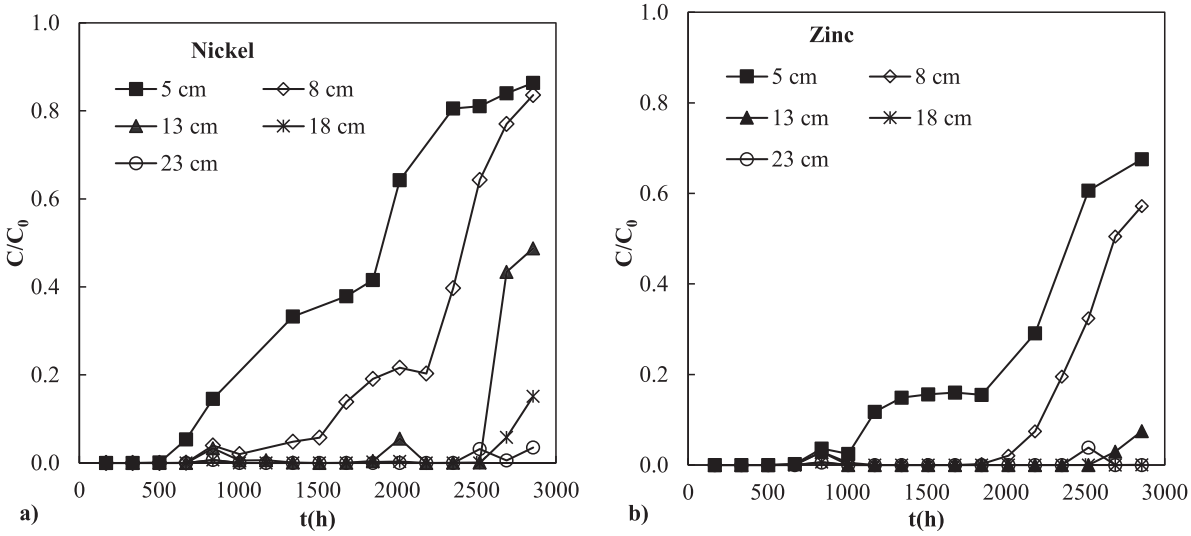

Fig. 4. Breakthrough curves of a) nickel and b) zinc at the sampling ports placed at a distance of 5, 8, 13, 18 and 23 cm from the inlet section of column A.

Fig. 5 shows the breakthrough curves for nickel and zinc at the sampling ports placed at a distance of 5, 8, 13, 18, 23 and 28 cm from the inlet section of column B.

For nickel removal (Fig. 5a), a thickness of almost 8 cm is necessary to remove the contaminant. The breakthrough time advances along the thickness of the reactive medium according to the process of exhaustion of the reactivity of the materials. The breakthrough time takes place simultaneously, after 672 h, considering the sampling ports placed at 18 (132 PVF), 23 (103 PVF) and 28 (85 PVF) cm from column inlet. The nickel removal efficiency exceeds 90 % up to 2520 h.

Zinc is removed from solution more easily than nickel (Fig. 5b) and its concentration, after 26 weeks (i.e. 4368 h) at 23 cm of thickness, is below the Italian regulatory limit. The breakthrough time observed at sampling ports located at 3 (i.e. 168 h, 198 PVF), 5 (i.e. 672 h, 475 PVF), 8 (i.e. 1512 h, 668 PVF), 13 (i.e. 2520 h, 686 PVF) and 18 cm (i.e. 3696 h, 726 PVF) linearly increases with the reactive medium thickness.

The concentration of copper remains below 1 mg/l in all sampling ports located after 3 cm (breakthrough curves not showed).

Fig. 6 shows the breakthrough curves of nickel (Fig. 6a) and zinc (Fig. 6b) derived from column test C.

The exhaustion of the reactive medium towards nickel removal (Fig. 6a), occurs in shorter times than in column A. This behavior is linked to the lower iron content per unit volume present in the first 4 cm of the reactive medium thickness. This rapid depletion of the reactivity is highlighted by the proximity of the breakthrough curves, which, for some thicknesses of the reactive medium tend

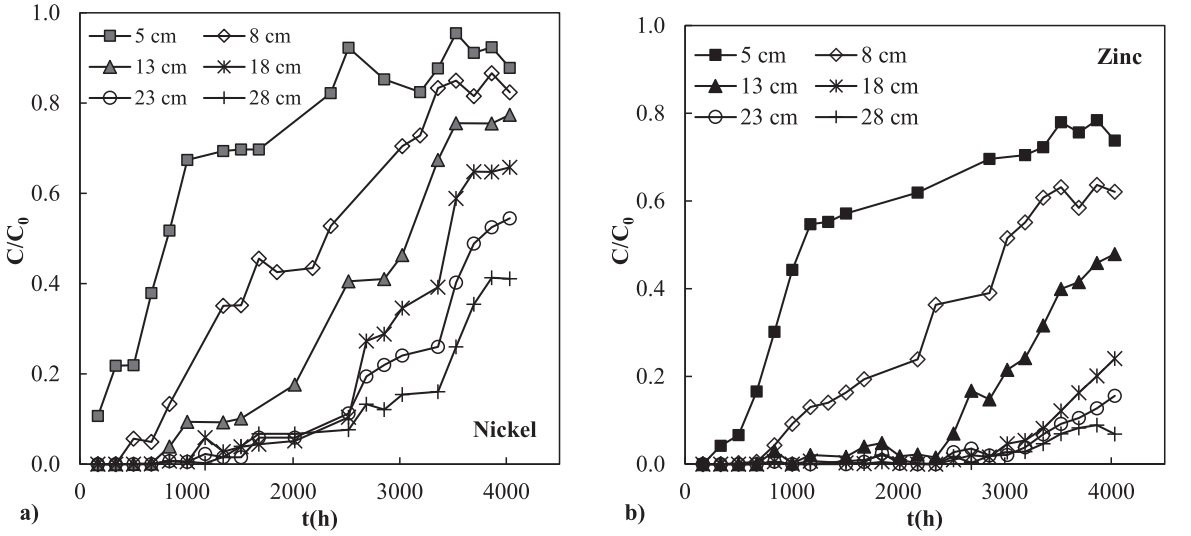

Fig. 5. Breakthrough curves of a) nickel and b) zinc at the sampling ports placed at a distance of 5, 8, 13, 18, 23 and 28 cm from the inlet section of column B.

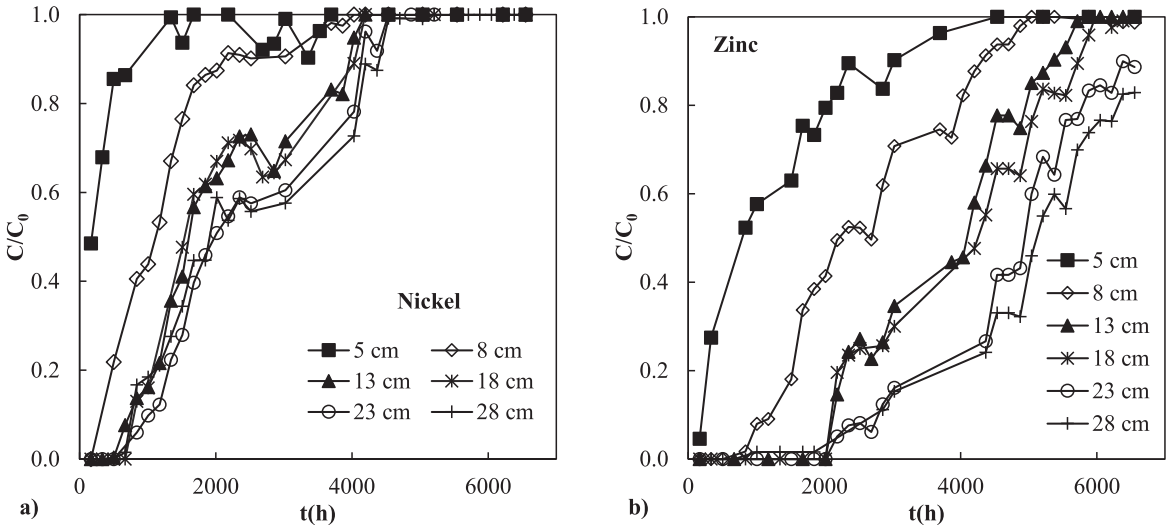

Fig. 6. Breakthrough curves of a) nickel and b) zinc at the sampling ports placed at a distance of 5, 8, 13, 18, 23 and 28 cm from the inlet section of column C.

to overlap, such as the breakthrough curves placed at L = 13 and L = 18 cm (breakthrough time equal to 504 h equivalent to 138 PVF for 13 cm and 99 PVF for 18 cm) or the breakthrough curves placed at L = 23 and L = 28 cm (breakthrough time equal to 672 h equivalent to 104 PVF for 23 cm and 85 PVF for 28 cm). The nickel removal efficiency exceeds 50 % up to 2000 h.

The breakthrough curves for zinc (Fig. 6b) are more widely spaced. In particular, the breakthrough time occurs after 1344 h at L = 8 cm (597 PVF), after 2184 h at L = 13 (597 PVF) and 18 cm (431 PVF) and after 2856 h at L = 23 (441 PVF) and 28 cm (362 PVF).

The concentration of copper remains below 1 mg/l in all sampling ports located after 3 cm (breakthrough curves not showed).

Fig. 7 shows the breakthrough time (y-axis) of nickel (Fig. 7a) and zinc (Fig. 7b) observed at each sampling port (x-axis) for the three columns. As previously observed in Figs. 4-6, it was not always possible to observe the breakthrough time in the first sampling ports. Fig. 7a shows that the breakthrough times do not always increase as the thickness increases. The observed profiles, which are different for the three columns, suggest the existence of an optimal thickness of the PRB for nickel removal. In particular, neglecting the hydraulic behavior (i.e. assuming that the hydraulic conductivity remains constant over time), an optimal thickness of the reactive medium, equal to 13, 18 and 23 cm can be identified for columns A, B, and C, respectively (Fig. 7a). The lower removal efficiency of the layers placed downstream from the inlet section could be attributed to the reduction in reactivity of the iron particles even in the absence of contaminants as also observed in previous studies (Madaffari et al., 2017). This behavior suggests that when ZVI is crossed by uncontaminated water, it is in any case corroded and this leads to a reduction in its reactivity over time.

Furthermore, it is necessary underline that the profiles observed in Fig. 7a are strictly linked to the regulatory limit, in this case equal to 0.02 mg/l.

For zinc (Fig. 7b), the breakthrough time linearly increases with the reactive medium thickness (data can be fitted with a linear equation having $R^2 > 0.87$).

The profiles of Fig. 7b can be used as design curves, if the hydraulic conductivity of the reactive medium remains constant over time. The thickness (i.e. the x-axis in Fig. 7b) of the PRB can be obtained if the volume of water to be treated and the flow rate entering the PRB are known.

To show more clearly the influence of the pre-treatment zone on the reactive behavior of a ZVI-based mixture, the results of the three columns are compared in Figs. 8 and 9 for nickel and zinc, at 18 and 23 cm of reactive medium thickness, respectively.

Considering 18 cm of reactive medium thickness (Fig. 8a), a substantial difference between the reactive behavior of column C with that of columns A and B towards nickel removal is observed. Although, this difference is reduced considering 23 cm of column length (Fig. 9a), it is possible to state that a content of iron lower than 20 % in volume in the first centimeters of the reactive medium can influence the reactivity towards nickel.

For zinc, the Italian regulatory limit at 18 cm of the reactive medium thickness is exceeded after 2000 and 3700 h passing from test C to test B, respectively. This difference between the breakthrough times is reduced considering 23 cm of column thickness (Fig. 8b and 9b). For column A, the limit was not reached in the period under study (17 weeks). Therefore, in terms of zinc removal, the iron content in the first centimeters of reactive medium thickness seems to reduce its influence as the thickness of the reactive medium increases.

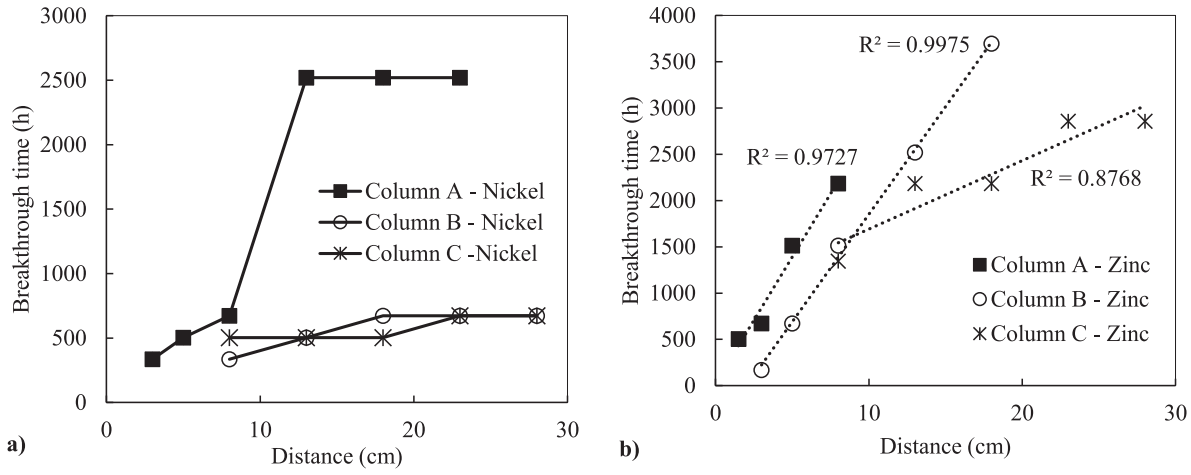

Fig. 7. Breakthrough times (h) vs. column distance (cm) for a) nickel and b) zinc.

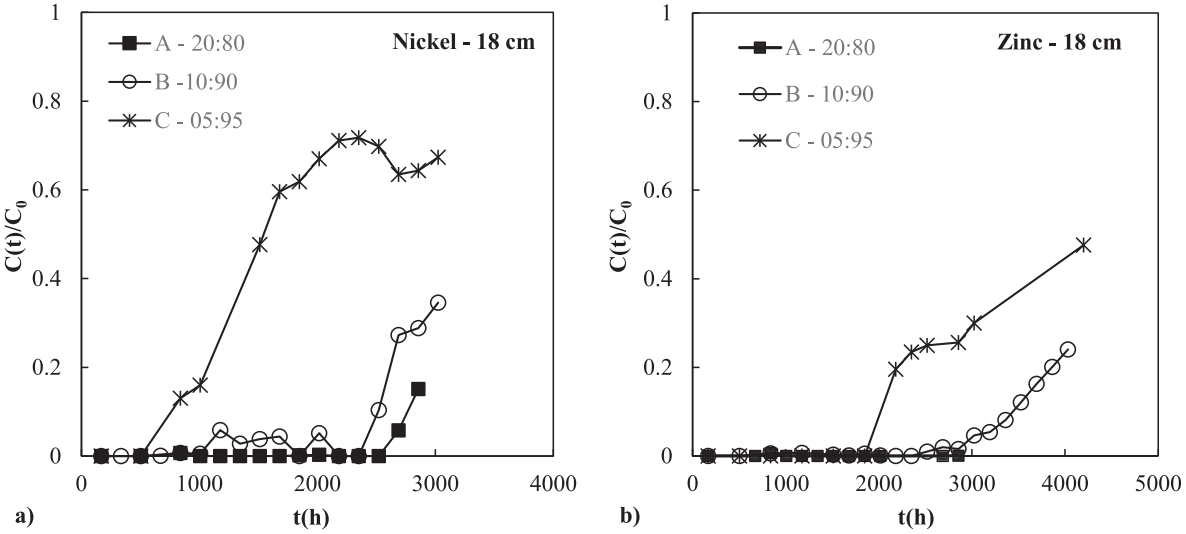

Fig. 8. Breakthrough curves of a) nickel and b) zinc at 18 cm for columns A, B and C.

3.3. Reactive and hydraulic lifetime

PRB lifetime is, in terms of reactivity, the length of time the system is able to maintain the concentration of the pollutant below the regulatory limit or, in terms of hydraulic conductivity, the time when groundwater flow is able to cross the barrier. Therefore, the longevity of the barrier will be established by examining the hydraulic and the reactive behavior of the three columns.

As far as the hydraulic behavior is concerned, the lifetime of the PRB was considered upon reaching a hydraulic conductivity value approximately one order of magnitude lower than the initial value. As regards reactive behavior, the lifetime of the PRB was considered upon reaching the maximum breakthrough time (with reference to the Italian regulatory limit).

In Table 2, for each column test, the event that could affect the lifetime (or longevity) of the reactive medium was identified both in terms of distance from the column inlet (or thickness of the reactive medium) and in terms of time during which the event was observed.

Assuming that a reduction in the hydraulic conductivity of one order of magnitude is not compatible with the correct operation of a PRB, column A would have required the substitution of the reactive medium after about 400 h. Considering the PRB thicknesses investigated in the tests, the maximum longevity for columns B and C is 672 h, which is the breakthrough time obtained for nickel. Therefore, from a comparison among the three tests, it emerges that the presence of the pretreatment zone increases barrier longevity by 68 %.

Neglecting the reactive behavior, column B would have required the substitution of the reactive medium after about 1500 h. Therefore, in this case, the presence of a pre-treatment area did not exclude the occurrence of clogging phenomena of the reactive medium but it did delay the

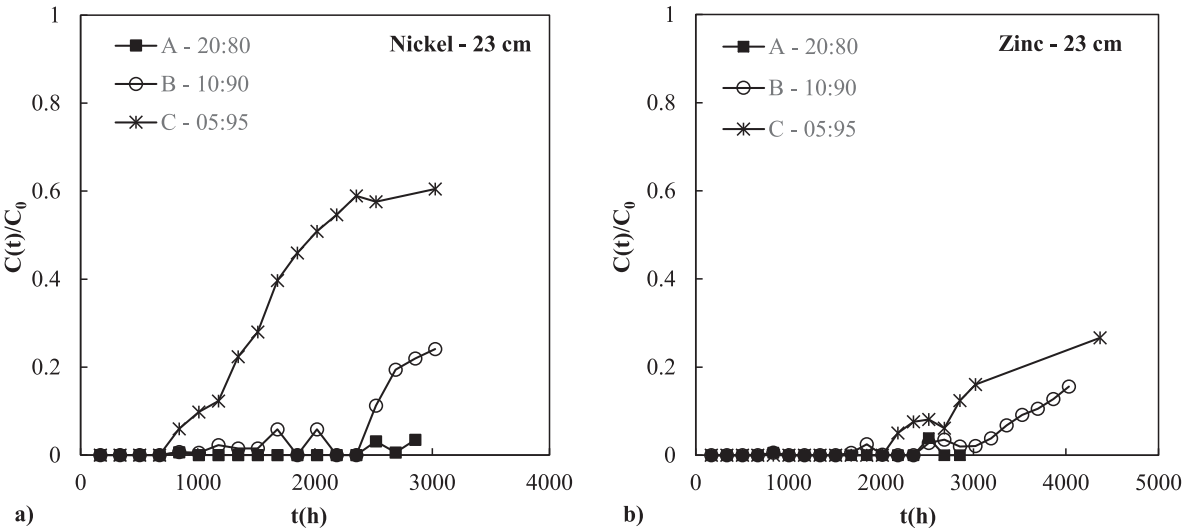

Fig. 9. Breakthrough curves of a) nickel and b) zinc at 23 cm for columns A, B and C.

Table 2
Time (t), pore volume of flow (PVF) and distance from column inlet (L) in which a hydraulic conductivity reduction of one order of magnitude or the contaminant breakthrough are observed.

ID	t [h]	PVF [-]	L [cm]	Event
A	400	467	3	Hydraulic conductivity reduction of one order of magnitude
	2184	957	8	Zinc breakthrough
	2520	679	13	Nickel breakthrough
	3144	3672	3	Copper breakthrough not observed until end of the test
B	1500	1768	3	Hydraulic conductivity reduction of one order of magnitude
	3696	4357	3	Copper breakthrough
	3696	726	18	Zinc breakthrough
	672	132	18	Nickel breakthrough
C	3528	4178	3	Copper breakthrough
	2856	441	23	Zinc breakthrough
	672	104	23	Nickel breakthrough
	7932	9395	3	Hydraulic conductivity remained constant until the end of the test

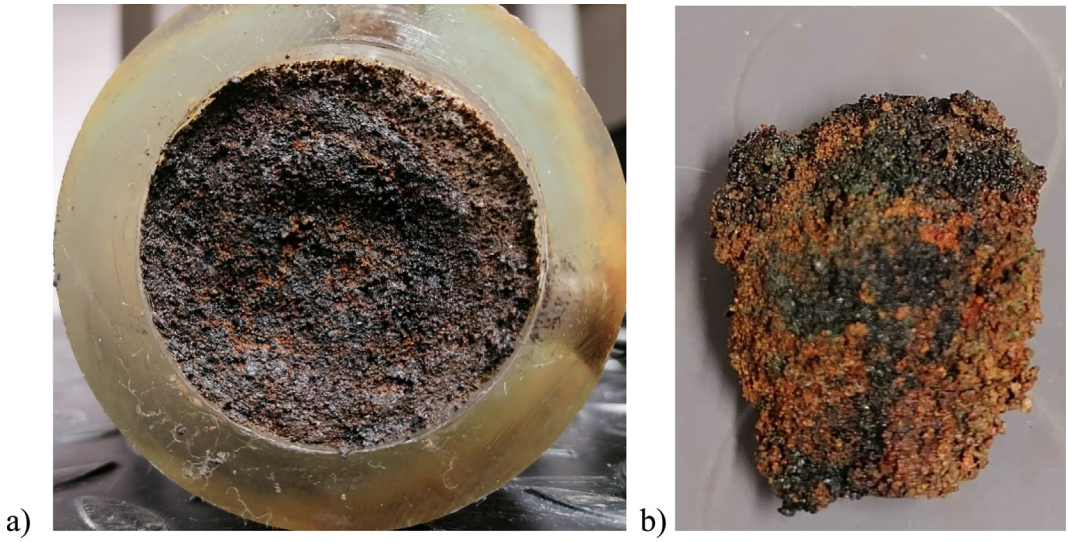

Fig. 10. ZVI/lapillus mixture inside column A after disassembly (Fig. 10a) and after extraction (Fig. 10b).

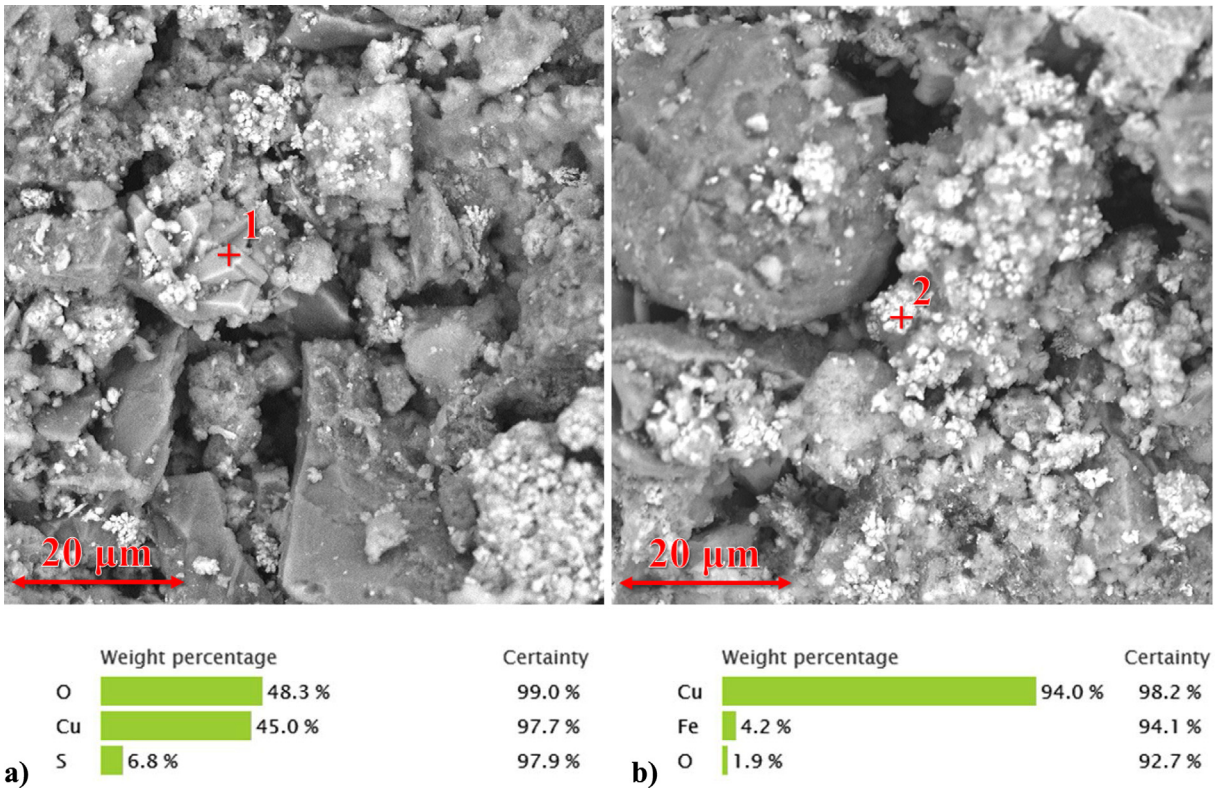

Fig. 11. SEM images of ZVI/lapillus mixture taken from column A and EDX analysis of (a) point 1 showing trapezoidal metallic copper and (b) point 2 showing a bulbous formation of copper.

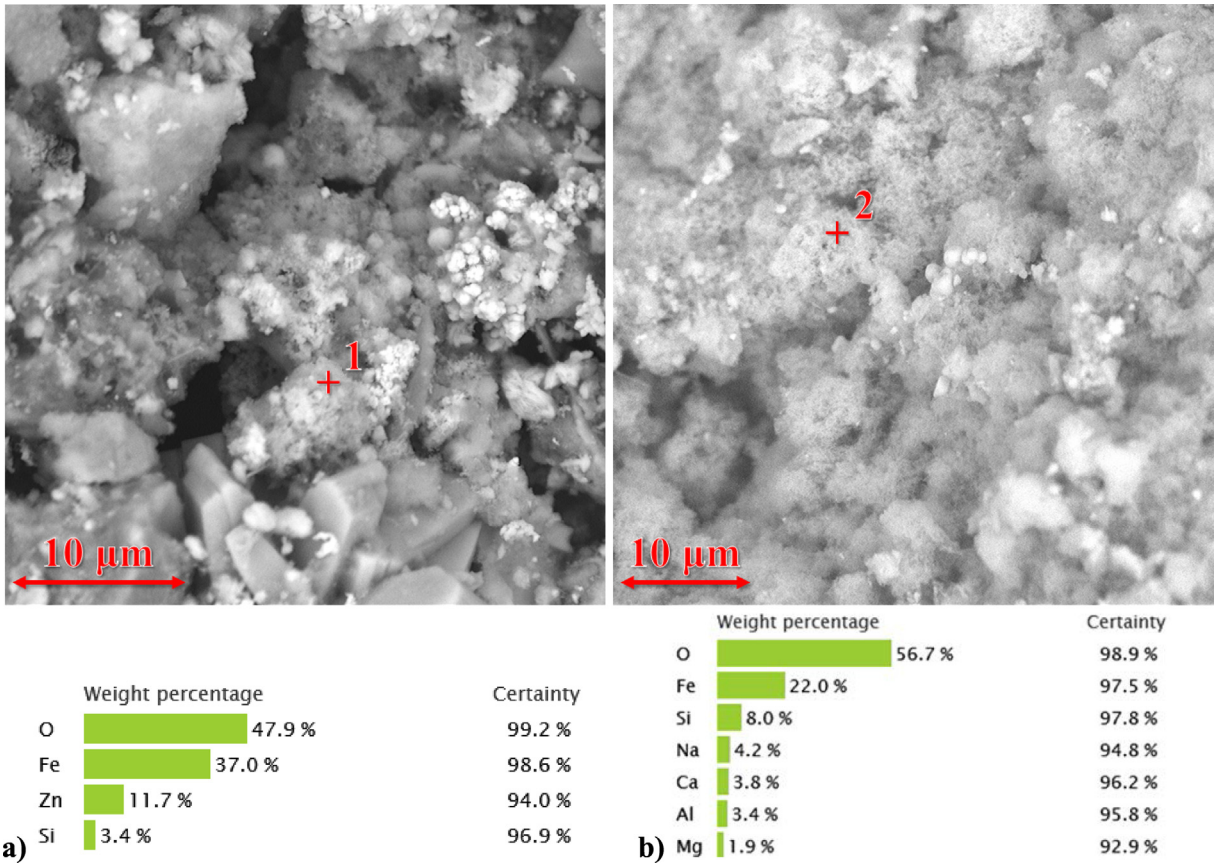

Fig. 12. SEM images of ZVI/lapillus mixture taken from a) column A and b) column B showing the spongeous nature of iron corrosion products and EDX analysis.

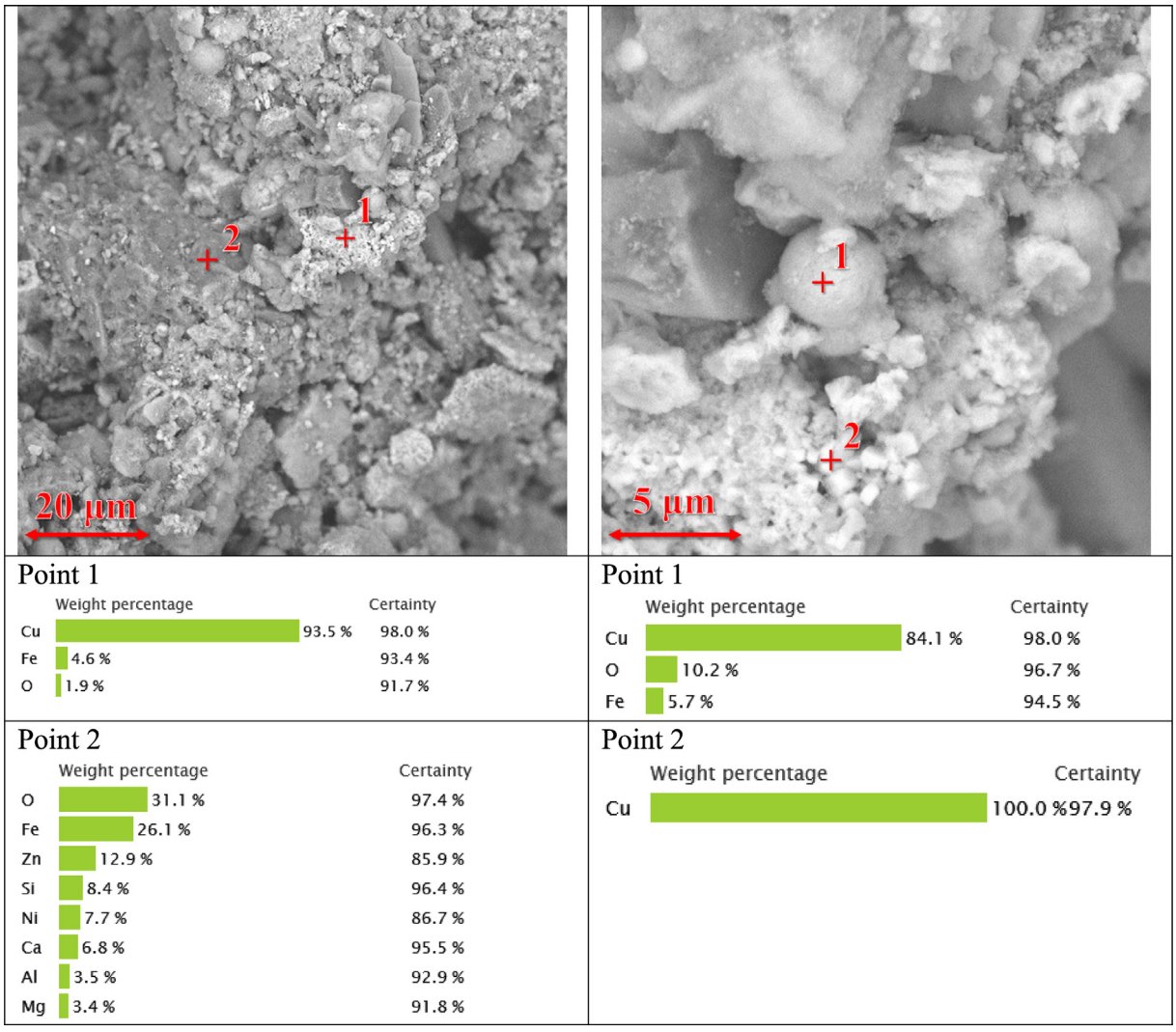

Fig. 14. SEM/EDX analyses of ZVI/Lapillus granular mixture taken from column C.

clogging phenomenon, increasing the longevity of the barrier by 275 %.

The lifetime of column C is linked to nickel removal and to the regulatory limit that must be reached, but the results highlighted in Fig. 7a show that an increase in the PRB thickness does not allow an increase in its longevity. In the absence of nickel, it is reasonable to assume that the longevity of column C is related to the removal of zinc and that it can be increased by increasing the thickness of the PRB (see design curves in Fig. 7b).

The study of the hydraulic and reactive behavior of the three configurations has shown that a pre-treatment zone increases the longevity of the PRB but it is necessary to design this zone by appropriately defining the iron dispersion rate and the thickness.

A PRB containing the pre-treatment zone can be easily installed using the caisson technology employed at Dover Air Force Base. In this case, a temporary divider was used to separate the pretreatment zone from the rest of the reactive medium during filling (Gavaskar et al., 2000).

The economic convenience of the proposed multilayer configuration lies in ensuring optimal long-term operation of the PRB, avoiding the much more expensive replacement of the reactive medium during the remediation treatment.

3.4. SEM-EDX analyses

Fig. 10 shows the material inside column A after disassembly (Fig. 10a) and a part of extracted material (Fig. 10b). The brown and gray areas represent lapillus and iron respectively. From Fig. 10b the aggregation/cementation among particles is clear.

SEM image of the reacted surface of the ZVI/lapillus granular mixture taken from the inlet of column A (Fig. 11) revealed the presence of copper in two different shapes. Trapezoidal copper crystals (point 1 of Fig. 11a) whose EDX analysis revealed the presence of 48.3 % of O, 45 % of Cu and 6.8 % of S (weight percent). The trapezoidal shape of deposited copper was also mentioned by (Komnitsas, 2007). In Fig. 11b copper can be found as a

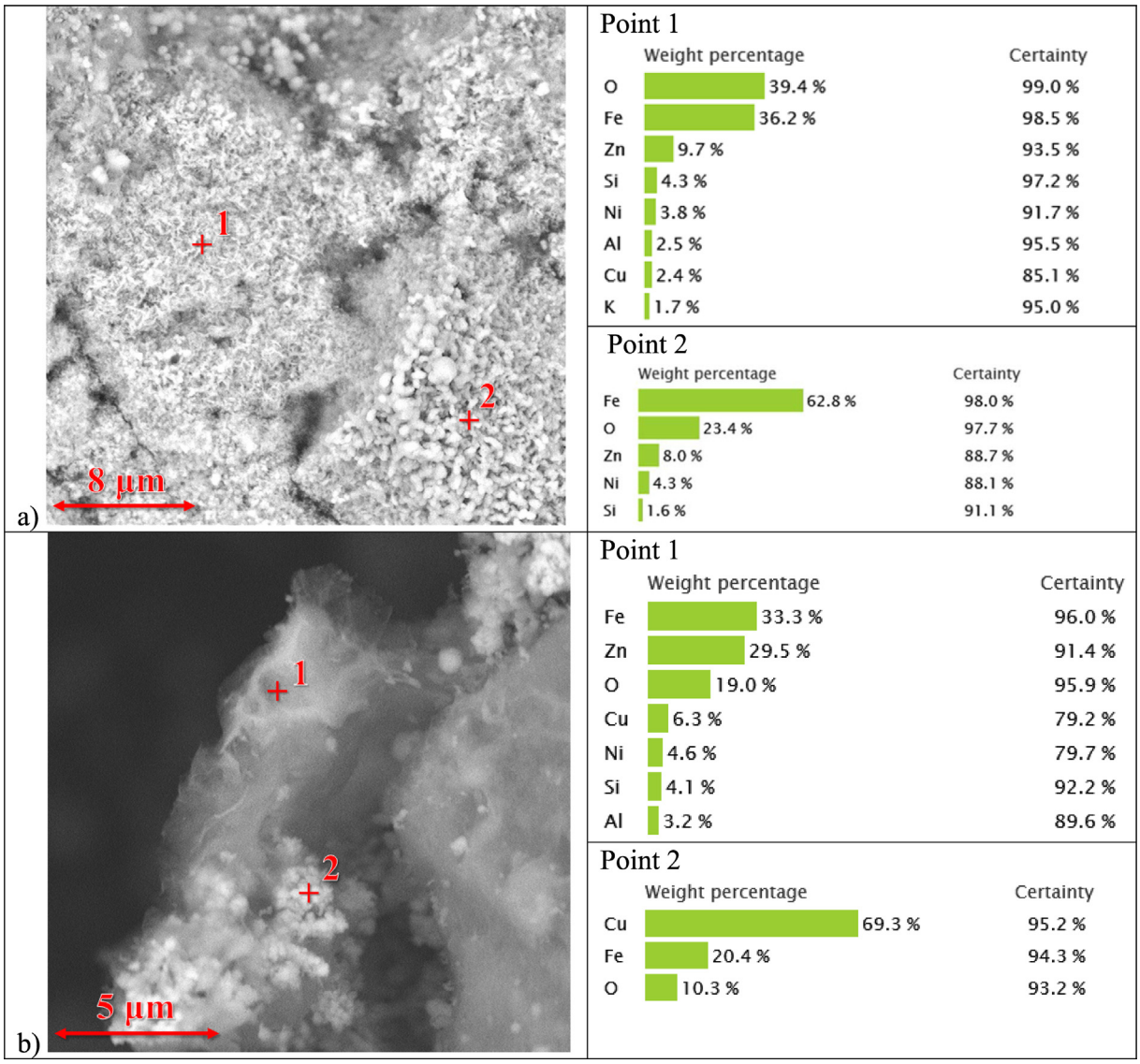

Fig. 13. SEM/EDX analyses of ZVI/Lapillus granular mixture taken from column B.

bulbous formation. EDX analysis performed at point 2 of Fig. 11b revealed the presence of 94 % of Cu, 4.2 % of Fe and 1.9 % of O (weight percent) and this is compatible with the reduction of Cu^{2+} to Cu^{0} (cementation process (Crane and Sapsford, 2018)). (Sánchez-España et al., 2022) also revealed this pseudo-spherical form of metallic copper produced by the cementation method.

Fig. 12 shows the SEM images of the ZVI/lapillus granular mixture taken from column A (Fig. 12a) and column B (Fig. 12b). From EDX analysis performed on points 1 and 2 of both figures, it is possible to hypothesize the presence of iron corrosion products with a spongeous nature. This morphology recalls the petal-shaped one revealed by Wang et al. (2007) or the amorphous form with a porous structure revealed by Fan et al. (2009).

EDX analysis performed on point 1 of Fig. 12a shows the presence of zinc most likely incorporated within iron corrosion products, this is compatible with adsorption and co-precipitation of zinc with iron hydroxide (Kishimoto et al., 2011).

Nickel was found mostly together with zinc, iron and oxygen as shown from SEM/EDX analyses of the granular mixture ZVI/lapillus taken from column B inlet (Fig. 13). The image depicted in Fig. 13a suggests a spongeous nature of the precipitates whereas higher magnification (Fig. 13b) clearly shows the presence of precipitates with a bulbous formation and containing copper, as shown previously, and a filamentous structure of precipitates containing Fe, O, Zn, Ni and Cu (this is compatible with adsorption and co-precipitation of the heavy metals with iron hydroxide).

SEM/EDX analyses of the ZVI/lapillus mixture taken from column C (Fig. 14) reveal the presence of precipitates containing copper with a bulbous formation, as previously observed in columns A or B, and precipitates of Fe and O (probably iron corrosion products) containing copper, nickel and zinc.

4. Conclusions

This research studied the behaviour of a PRB configuration composed of two layers of a granular mixture of ZVI and lapillus, each characterized by a different degree of iron dispersion. The objective of the first layer, named "pre-treatment layer" where ZVI particles are more widely dispersed, is to avoid the clogging phenomenon. To explore the effectiveness of this multi-layer configuration three column tests were performed. Two columns were filled with an initial 4-cm-thick layer consisting of a ZVI/lapillus granular mixture with a volumetric ratio of 10:90 (Column B) or 5:95 (Column C) and a second layer with a volumetric ratio equal to 20:80. A third column filled with a single layer of the 20:80 ZVI/lapillus mixture was used as a benchmark (Column A). The columns were permeated with a multi-contaminated solution of copper, nickel and zinc.

Column A showed the lowest longevity due to a rapid reduction in the hydraulic conductivity starting at the inlet section of the column (decrease of one order of magnitude after 400 h) and propagating up to the second layer (decrease of one order of magnitude after 1600 h). The hydraulic conductivity reduction of one order of magnitude was also observed in the first layer of column B after 1500 h. In column C for the duration of the test (at least 8 months) the permeability remained constant.

The longevity of columns B and C was linked to nickel removal, in these two columns the presence of the pre-treatment layer allowed an increase in PRB longevity of 68 % compared to column A.

In the three columns, copper and zinc were removed for longer period than nickel and the breakthrough time generally increased with barrier thickness. For nickel, an optimal thickness of the PRB equal to 13, 18 and 23 cm for column A, B, and C respectively was identified. In this case, an increase in the thickness of the reactive medium did not correspond to a significant removal of the contaminant.

In cases where breakthrough times increase linearly with reactive medium thickness and hydraulic conductivity remains constant over time, PRB longevity can be increased by increasing PRB thickness. In this case, design curves can be drawn, as proposed in this study, in order to establish the thickness of the PRB according to the in situ conditions (i.e. volume of water to be treated and flow rate entering the PRB).

SEM-EDX analyses of the reacted surface of the ZVI/lapillus granular mixture taken from the column inlet, revealed the presence of copper as trapezoidal crystals or bulbous formation, the presence of iron corrosion products with a spongeous nature, and the presence of nickel and zinc most likely incorporated within iron corrosion products.

References

Bartlett, T., 2005. Variation in Hydraulic Conductivity Over Time at the Monticello Permeable Reactive Barrier 1–405.

Bilardi, S., Calabró, P.S., Moraci, N., 2015. Simultaneous removal of CU II, NI II and ZN II by a granular mixture of zero-valent iron and pumice in column systems. Desalin. Water Treat. 55, 767–776. https://doi.org/10.1080/19443994.2014.916234.

Bilardi, S., Calabrò, P.S., Moraci, N., 2019. The removal efficiency and long-term hydraulic behaviour of zero valent iron/lapillus mixtures for the simultaneous removal of Cu2+, Ni2+ and Zn2+. Sci. Total Environ. 675, 490–500. https://doi.org/10.1016/j.scitotenv.2019.04.260.

Bilardi, S., Calabrò, P.S., Moraci, N., Madaffari, M.G., Ranjbar, E., 2020. A comparison between Fe 0 /pumice and Fe 0 /lapillus mixtures in permeable reactive barriers. Environ. Geotech. 7, 524–539. https://doi.org/10.1680/jenge.17.00095.

Bilardi, S., Calabrò, P.S., Moraci, N., 2023. A Review of the Hydraulic Performance of Permeable Reactive Barriers Based on Granular Zero Valent Iron. Water 15, 200. https://doi.org/10.3390/w15010200.

Calabrò, P.S., Bilardi, S., Moraci, N., 2021. Advancements in the use of filtration materials for the removal of heavy metals from multicontaminated solutions. Curr. Opin. Environ. Sci. Heal. 20. https://doi.org/10.1016/j.coesh.2021.100241 100241.

Cao, V., Ndé-Tchoupé, A.I., Hu, R., Gwenzi, W., Noubactep, C., 2021. The mechanism of contaminant removal in Fe(0)/H2O systems: The burden of a poor literature review. Chemosphere 280. https://doi.org/10.1016/j.chemosphere.2021.130614 130614.

Crane, R.A., Sapsford, D.J., 2018. Selective formation of copper nanoparticles from acid mine drainage using nanoscale zerovalent iron particles. J. Hazard. Mater. https://doi.org/10.1016/j.jhazmat.2017.12.014.

Fan, X., Guan, X., Ma, J., Ai, H., 2009. Kinetics and corrosion products of aqueous nitrate reduction by iron powder without reaction conditions control. J. Environ. Sci. https://doi.org/10.1016/S1001-0742(08)62378-5.

Fu, F.L., Dionysiou, D.D., Liu, H., 2014. The use of zero-valent iron for groundwater remediation and wastewater treatment: A review. J. Hazard. Mater. 267, 194–205. https://doi.org/10.1016/j.jhazmat.2013.12.062.

Gavaskar, A., Gupta, N., Sass, B., Yoon, W.-S., Janosy, R., 2000. Design, Construction, and Monitoring of the Permeable Reactive Barrier in Area 5 at Dover Air Force Base 399.

Henderson, A.D., Demond, A.H., 2007. Long-Term Performance of Zero-Valent Iron Permeable Reactive Barriers: A Critical Review. Environ. Eng. Sci. 24, 401–423. https://doi.org/10.1089/ees.2006.0071.

Hu, N., 2019. Redirecting Research on Fe0 for Environmental Remediation: The Search for Synergy. Int. J. Environ. Res. Public Health 16, 4465. https://doi.org/10.3390/ijerph16224465.

Hu, R., Cui, X., Gwenzi, W., Wu, S., Noubactep, C., 2018. Fe0/H2O Systems for Environmental Remediation: The Scientific History and Future Research Directions. Water 10, 1739. https://doi.org/10.3390/w10121739.

Hu, R., Yang, H., Tao, R., Cui, X., Xiao, M., Amoah, B.K., Cao, V., Lufingo, M., Soppa-Sangue, N.P., Ndé-Tchoupé, A.I., Gatcha-Bandjun, N., Sipowo-Tala, V.R., Gwenzi, W., Noubactep, C., 2020. Metallic Iron for Environmental Remediation: Starting an Overdue Progress in Knowledge. Water 12, 641. https://doi.org/10.3390/w12030641.

ITRC, 2011. Permeable Reactive Barrier: Technology Update PRB-5, Interstate Technology & Regulatory Council.

Kishimoto, N., Iwano, S., Narazaki, Y., 2011. Mechanistic Consideration of Zinc Ion Removal by Zero-Valent Iron. Water, Air, Soil Pollut. 221, 183–189. https://doi.org/10.1007/s11270-011-0781-1.

Komnitsas, K., 2007. Long-term efficiency and kinetic evaluation of ZVI barriers during clean-up of copper containing solutions 20, 1200–1209. https://doi.org/10.1016/j.mineng.2007.05.002.

Lee, J.Y., Lee, K.J., Youm, S.Y., Lee, M.R., Kamala-Kannan, S., Oh, B. T., 2010. Stability of multi-permeable reactive barriers for long term removal of mixed contaminants. Bull. Environ. Contam. Toxicol. https://doi.org/10.1007/s00128-009-9918-y.

Li, L., Benson, C.H., 2010. Evaluation of five strategies to limit the impact of fouling in permeable reactive barriers. J. Hazard. Mater. 181, 170–180. https://doi.org/10.1016/j.jhazmat.2010.04.113.

Limper, D., Fellinger, G.P., Ekolu, S.O., 2018. Evaluation and microanalytical study of ZVI/scoria zeolite mixtures for treating acid mine drainage using reactive barriers - Removal mechanisms. J. Environ. Chem. Eng. https://doi.org/10.1016/j.jece.2018.08.064.

Madaffari, M.G., Bilardi, S., Calabrò, P.S., Moraci, N., 2017. Nickel removal by zero valent iron/lapillus mixtures in column systems. Soils Found. 57, 745–759. https://doi.org/10.1016/j.sandf.2017.08.006.

Makota, S., Nde-Tchoupe, A.I., Mwakabona, H.T., Tepong-Tsindé, R., Noubactep, C., Nassi, A., Njau, K.N., 2017. Metallic iron for water treatment: leaving the valley of confusion. Appl. Water Sci. https://doi.org/10.1007/s13201-017-0601-x.

Moraci, N., Bilardi, S., Calabrò, P.S., 2015. Design of permeable reactive barriers for remediation of groundwater contaminated by heavy metals. Riv. Ital. Di Geotec. 49, 59–86.

Moraci, N., Bilardi, S., Calabrò, P.S., 2017. Fe 0 /pumice mixtures: from laboratory tests to permeable reactive barrier design. Environ. Geotech. 4, 245–256. https://doi.org/10.1680/jenge.15.00002.

Moraci, N., Bilardi, S., Mandaglio, M.C., 2022. Factors affecting geotextile filter long-term behaviour and their relevance in design. Geosynth. Int. 29, 19–42. https://doi.org/10.1680/jgein.21.00019.

Morrison, S., 2003. Performance evaluation of a permeable reactive barrier using reaction products as tracers. Environ. Sci. Technol. 37, 2302–2309. https://doi.org/10.1021/es0209565.

Obiri-Nyarko, F., Grajales-Mesa, S.J., Malina, G., 2014. An overview of permeable reactive barriers for in situ sustainable groundwater remediation. Chemosphere 111, 243–259. https://doi.org/10.1016/j.chemosphere.2014.03.112.

Pawluk, K., Fronczyk, J., 2015. Evaluation of single and multilayered reactive zones for heavy metals removal from stormwater. Environ. Technol. 36, 1576–1583. https://doi.org/10.1080/09593330.2014.997299.

Pawluk, K., Fronczyk, J., Garbulewski, K., 2019. Experimental development of contaminants removal from multicomponent solutions using ZVI, zeolite and modified construction aggregate – batch and column tests. Desalin. Water Treat. https://doi.org/10.5004/dwt.2019.23544.

Phillips, D.H., Nooten, T.V., Bastiaens, L., Russell, M.I., Dickson, K., Plant, S., Ahad, J.M.E., Newton, T., Elliot, T., Kalin, R.M., 2010. Ten Year Performance Evaluation of a Field-Scale Zero-Valent Iron Permeable Reactive Barrier Installed to Remediate Trichloroethene Contaminated Groundwater. Environ. Sci. Technol. 44, 3861–3869. https://doi.org/10.1021/es902737t.

Połoński, M., Pawluk, K., Rybka, I., 2017. Optimization Model for the Design of Multi-layered Permeable Reactive Barriers, in: IOP Conference Series: Materials Science and Engineering. https://doi.org/10.1088/1757-899X/245/7/072017.

Rajendran, S., Priya, T.A.K., Khoo, K.S., Hoang, T.K.A., Ng, H.S., Munawaroh, H.S.H., Karaman, C., Orooji, Y., Show, P.L., 2022. A critical review on various remediation approaches for heavy metal contaminants removal from contaminated soils. Chemosphere. https://doi.org/10.1016/j.chemosphere.2021.132369.

Ruhl, A.S., Franz, G., Gernert, U., Jekel, M., 2014. Corrosion product and precipitate distribution in two-component Fe(0) permeable reactive barriers. Chem. Eng. J. 239, 26–32. https://doi.org/10.1016/j.cej.2013.11.017.

Sánchez-España, J., Ilin, A., Yusta, I., 2022. Metallic Copper (Cu[0]) Obtained from Cu2+-Rich Acidic Mine Waters by Two Different Reduction Methods: Crystallographic and Geochemical Aspects. Minerals. https://doi.org/10.3390/min12030322.

Singh, R., Chakma, S., Birke, V., 2020. Numerical modelling and performance evaluation of multi-permeable reactive barrier system for aquifer remediation susceptible to chloride contamination. Groundw. Sustain. Dev. https://doi.org/10.1016/j.gsd.2019.100317.

Thakur, A.K., Vithanage, M., Das, D.B., Kumar, M., 2020. A review on design, material selection, mechanism, and modelling of permeable reactive barrier for community-scale groundwater treatment. Environ. Technol. Innov. 19. https://doi.org/10.1016/j.eti.2020.100917 100917.

Ullah, S., Guo, X., Luo, X., Zhang, X., Li, Y., Liang, Z., 2020b. The coupling of sand with ZVI/oxidants achieved proportional and highly efficient removal of arsenic. Front. Environ. Sci. Eng. https://doi.org/10.1007/s11783-020-1273-6.

Ullah, S., Faiz, P., Leng, S., 2020a. Synthesis, Mechanism, and Performance Assessment of Zero-Valent Iron for Metal-Contaminated Water Remediation: A Review. Clean - Soil, Air, Water. https://doi.org/10.1002/clen.202000080.

Wang, Z., Xu, C., Cao, X., Xu, B., 2007. The Morphology, Phase Composition and Effect of Corrosion Product on Simulated Archaeological Iron. Chinese J. Chem. Eng. 15, 433–438. https://doi.org/10.1016/S1004-9541(07)60104-9.

Wilkin, R.T., Acree, S.D., Ross, R.R., Puls, R.W., Lee, T.R., Woods, L. L., 2014. Fifteen-year assessment of a permeable reactive barrier for treatment of chromate and trichloroethylene in groundwater. Sci. Total Environ. 468–469, 186–194. https://doi.org/10.1016/j.scitotenv.2013.08.056.

Xu, Z., Wu, Y., Yu, F., 2012. A Three-Dimensional Flow and Transport Modeling of an Aquifer Contaminated by Perchloroethylene Subject to Multi-PRB Remediation. Transp. Porous Media 91, 319–337. https://doi.org/10.1007/s11242-011-9847-1.

Yang, H., Liu, Q., Hu, R., Ptak, T., Taherdangkoo, R., Liu, Y., Noubactep, C., 2022. Numerical case studies on long-term effectiveness of metallic iron based permeable reactive barriers: Importance of porosity heterogeneity of the barrier. J. Hydrol. 612. https://doi.org/10.1016/j.jhydrol.2022.128148 128148.

Yang, Z., Shan, C., Zhang, W., Jiang, Z., Guan, X., Pan, B., 2016. Temporospatial evolution and removal mechanisms of As(V) and Se (VI) in ZVI column with H2O2 as corrosion accelerator. Water Res. 106, 461–469. https://doi.org/10.1016/j.watres.2016.10.030.

Ye, J., Chen, X., Chen, C., Bate, B., 2019. Emerging sustainable technologies for remediation of soils and groundwater in a municipal solid waste landfill site – A review. Chemosphere 227, 681–702. https://doi.org/10.1016/j.chemosphere.2019.04.053.

Zhu, F., Tan, X., Zhao, W., Feng, L., He, S., Wei, L., Yang, L., Wang, K., Zhao, Q., 2022. Efficiency assessment of ZVI-based media as fillers in permeable reactive barrier for multiple heavy metal-contaminated groundwater remediation. J. Hazard. Mater. https://doi.org/10.1016/j.jhazmat.2021.127605.